Modeling and measurements on an obstructed glow discharge in helium

Z. Donkó and K. Rózsa
Research Institute for Solid State Physics, P.O. Box 49, H-1525 Budapest, Hungary

R. C. Tobin
Monash University, Clayton, Victoria 3168, Australia

K. A. Peard
Victoria University of Technology, Footscray, Victoria 3011, Australia
(Received 23 September 1993)

An obstructed glow discharge in helium has been ivestigated both experimentally and by means of a Monte Carlo simulation. The voltage-current characteristics of the discharge have been measured and the spatial distribution of the electric field between the electrodes was determined using Stark spectroscopy. The electric field distribution was also determined by a self-consistent calculation and the results show good agreement with data obtained from Stark measurements. Other discharge parameters (electron multiplication data, energy distribution of electrons absorbed by the anode, energy distribution of ionizing electrons, share of high-energy electrons in ion production, and spatial distribution of ion production) were obtained from the modeling calculations to provide detailed insight into the discharge operation. The effect of the electrode reflection of electrons on the discharge characteristics was also investigated.

PACS number(s): 52.80.Hc, 51.50.+v

I. INTRODUCTION

The obstructed regime of glow discharges has been of interest from the early decades of this century [1–4] up to recent years [5,6]. Recently, obstructed discharges have found increased application to the design of hollow cathode lasers and of high voltage switches. A more quantitative understanding of this type of discharge than is currently available would facilitate these designs.

The usual definition of the obstructed discharge is given in terms of reducing the electrode separation (or gas pressure) in a glow discharge [3,4]. When the separation is decreased to a value somewhat longer than the cathode dark space, the discharge voltage begins to rise. This effect is more pronounced if the cathode-anode separation is further decreased.

We have investigated an obstructed discharge in helium gas, both experimentally and by means of a Monte Carlo simulation. The voltage-current characteristics of the discharge have been measured and the spatial distribution of the electric field was determined using Stark spectroscopy on traces of hydrogen gas in the discharge. From the model of the discharge, we have obtained the self-consistent electric field distribution in the discharge gap, electron multiplication data, energy distribution of electrons absorbed by the anode, energy distribution of ionizing electrons, share of high-energy electrons in ion production, and spatial distribution of ion production.

These characteristics of the discharge in the obstructed regime were calculated at different gas pressures. The Stark measurements of the electric field confirmed the results of the self-consistent electric field calculations.

II. EXPERIMENT

The experimental discharge tube (see Fig. 1) had two graphite electrodes of 20 mm diameter separated by 4.6 mm. A 20.6-mm inner-diameter metal tube at floating potential limited the space for the discharge. The separation of the electrodes and the 0.3-mm gap between the tube and the electrodes were maintained by ceramic spacers. The metal tube had eight narrow slits of 0.2 mm width equally spaced at 0.6 mm from each other. These slits allowed a spatially resolved spectroscopic investigation of the discharge. This arrangement defined the volume of the discharge and allowed the study of the optical spectrum, despite the deposition of the sputtered cathode material.

The experimental setup used in the electric field measurements is shown in Fig. 2. Light emitted from the discharge was introduced into the entrance slit of a Zeiss

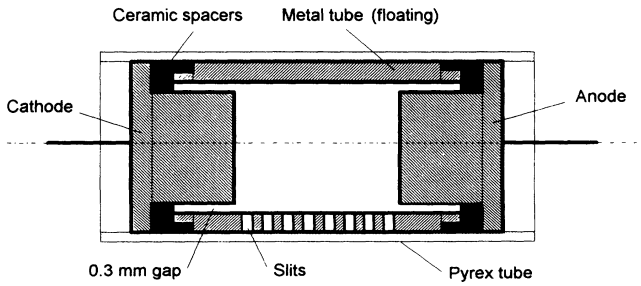

FIG. 1. Scheme of the experimental discharge tube. (Dimensions are not to scale.)

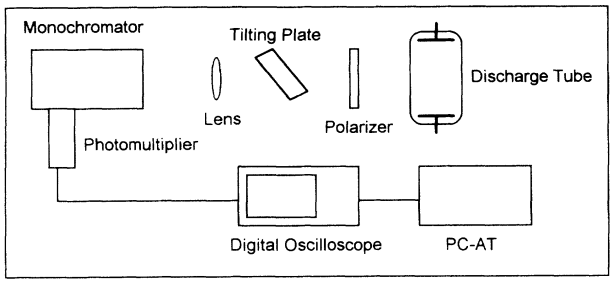

FIG. 2. Experimental setup for Stark line-shape measurements.

PGS-2 monochromator having a focal length of 2 m and a resolution better than 0.01 nm in the first order. The P and S polarization components of the split spectral line were selected by a polarizer. The axial distribution of the discharge was scanned by tilting a plane parallel quartz plate. Since the discharge tube inevitably contained traces of hydrogen, the field measurements were carried out by recording the line shape of the H_δ spectral line ($\lambda=401.2$ nm). The use of hydrogen lines for field measurement is common [6–8] because its Stark effect is linear and well understood [9], so that the measured data can be relatively easily interpreted.

To record the line shapes, the monochromator was slowly tuned over the examined spectral line by a stepping motor (approximately 2 sec/step). The signal from the photomultiplier was fed to a Hewlett Packard Model 54501A digitizing oscilloscope and transferred to a PC/AT computer. In this way the line shape was obtained in the form of a data vector consisting of intensity values at spectral positions $\lambda_k=\lambda_0+k\Delta\lambda_0$ ($k=0,1,2,\ldots$) uniformly separated by $\Delta\lambda_0=0.0059$ nm (λ_0 corresponds to the start of the recording). For the data acquisition, we assumed that the observed line shape is a result of simultaneous effects of Doppler broadening and Stark splitting, and is also affected by the transfer function of the monochromator.

The unsplit spectral lines were assumed to have a temperature- (T_g) dependent Gaussian line shape $D(\Delta\lambda,T_g)$. The transfer function of the monochromator, $T(\Delta\lambda)$, was measured using a He-Ne laser. The "Stark pattern" [$S(\Delta\lambda,E)$, the position and relative amplitude of the split spectral components, which depend on the electric field strength E] were taken from theoretical calculations [10]. Having measured $T(\Delta\lambda)$, for any T_g and E we were able to calculate the triple convolution $R(\Delta\lambda,T_g,E)=D(\Delta\lambda,T_g)\circ T(\Delta\lambda)\circ S(\Delta\lambda,E)$. For T_g and E values, approximating the experimental conditions $R(\Delta\lambda,T_g,E)$ looks "similar" to the measured line shape. R was calculated with the same $\Delta\lambda_0$ resolution with which the experimental data were obtained, its values were determined at the $\Delta\lambda_k=k\Delta\lambda_0$ ($k=0,\pm1,\pm2,\ldots$) points. In order to be able to fit the theoretical line-shape data $R(\Delta\lambda_k=k\Delta\lambda_0,T_g,E)$ to the data corresponding to the measured line shape, we had to shift R in wavelength by $\Delta\lambda_s=s\Delta\lambda_0$ (to match to the position of experimental data) and multiply it by an amplitude factor α (to match in amplitude). The shift (s) and amplitude factor (α) introduced were also fitting parameters like T_g and E. In this way, four parameters were used in the fitting of the measured and theoretical data vectors, the similarity of which was measured by an error function,

$$h(T_g,E,s,\alpha)=\sum_i (M_i-R_i')^2 ,$$

where M_i and R_i' are the elements of the measured data vector, and the shifted and amplitude corrected R data vector, respectively. Our aim to minimize h has been done by using a random optimization procedure in which the fitting parameters ($T_g E,s,\alpha$) were randomly modified (one at a time) and the new parameter values were accepted whenever they resulted in a smaller h than the previously accepted parameters.

III. THE MODELING OF THE DISCHARGE

In the modeling we assumed a radially uniform discharge between two plane electrodes. No edge effects were taken into account. Thus, the spatially resolved discharge characteristics are only functions of the spatial coordinate x measured from the cathode. However, the electrons are traced in the three-dimensional space, which provides a quite realistic description of their motion [11].

As high values of E/n (electric field to gas density ratio) and the presence of boundaries induce nonequilibrium effects in the motion of electrons [12,13], Monte Carlo simulation was applied to follow the trajectories of electrons in the discharge gap. Single electrons were released from the cathode of the discharge and their path was followed as they participated in the collision processes. The free path of each electron between successive collisions, as well as the type of the collisions that actually occurs after a free path, are assigned based on random numbers [11]. Finally, the electrons were absorbed by the cathode or by the anode. In most of our studies, the cathode and anode electrodes were assumed to be perfectly absorbing but the effect of electron reflection was also studied. All the secondary electrons created in ionizing collisions were traced in the simulation.

The initial energy of each electron emitted from the cathode was randomly chosen to be between 0 eV and $E_i-2\varphi$, where E_i is the ionization potential of the gas and φ is the work function of the cathode material [14].

The following elementary processes were taken into account in the model: elastic scattering of electrons from He atoms, electron impact excitation of He atoms, and electron impact ionization of He atoms.

The elastic scattering of electrons was assumed to be anisotropic. Whereas high-energy electrons were more likely to be scattered in the forward direction, the scattering is more isotropic in the case of low electron energies [15]. The energy loss of electrons in elastic scattering was neglected. In the case of electron impact excitation, isotropic scattering using a total cross section for excitation was applied, i.e., no specific energy levels of the atom were distinguished. The incoming electron could lose an energy randomly chosen between the energy of the first

excited level and the ionization level. In the electron impact ionization process, the trajectories of incoming, scattered, and ejected electrons were assumed to lie in one plane. The scattered and ejected electrons shared the remaining kinetic energy randomly, the directions of their velocity vectors being mutually perpendicular [11].

Measured cross sections were used for all elementary processes [16,17]. No ionization from the metastable and from other excited levels was taken into account due to the low current density. Because of the high electric field, volume recombination was neglected.

The input data of the model are the gas pressure and the experimentally determined voltage and current density of the discharge. The discharge gap was resolved into a number of divisions (typically $N=20-30$). In each of these divisions, a linearly decreasing electric field was assumed and the electrons were traced by the method described in detail in [11].

In an iterative method the $E(x)$, the electric field distribution (the electric field at the boundaries of the divisions) was determined in a self-consistent way. First, a linear decrease of the field from the cathode to the anode was assumed. A given number of electrons were emitted from the cathode one by one and they were traced in this field distribution by the Monte Carlo simulation procedure. Having traced a sufficient number of electrons, the electron energy distribution is readily obtained [11]. These data can be used to calculate the average velocity of electrons: $\langle v_e(x)\rangle$. The average velocity of the He^+ ions is calculated, based on the equilibrium assumption [18], from

$$\langle v_i(x)\rangle=\sqrt{2eE(x)/Mn\pi\sigma}\ , \tag{1}$$

where e is the charge of the electron, M the ion mass, n the gas density, and σ is the cross section of the symmetric charge exchange collision $He^+ + He \rightarrow He + He^+$. Since σ depends on the ion energy (or velocity)

$$\sigma=k_1-k_2\ln[\langle v_i(x)\rangle]\ , \tag{2}$$

where k_1 and k_2 are constants to a good approximation [19–21], the average ion velocity $\langle v_i(x)\rangle$ can be found by solving (1) and (2) simultaneously.

The fluxes of electrons $[F_e(x)]$ and He^+ ions $[F_i(x)]$ per emitted electron are also obtained from the simulation. As the current density j is known from the experiment, the normalized current density taken by electrons (j_e) and by He^+ ions (j_i) can be calculated,

$$j_e(x)=jF_e(x)/[F_e(x)+F_i(x)]\ , \tag{3a}$$

$$j_i(x)=jF_i(x)/[F_e(x)+F_i(x)]\ . \tag{3b}$$

The space charge densities are given by

$$\rho_e(x)=j_e(x)/\langle v_e(x)\rangle\ , \tag{4a}$$

$$\rho_i(x)=j_i(x)/\langle v_i(x)\rangle\ . \tag{4b}$$

The electric field distribution can be found by using the Poisson equation (neglecting the negative space charge),

$$dE/dx=-\rho_i/\varepsilon\ , \tag{5}$$

and taking into account that the electric field obeys the condition

$$\int_{x=0}^{L}E(x)dx=V\ , \tag{6}$$

where V is the discharge voltage and L is the electrode separation.

The modification of the original electric field due to the space charge is calculated and in the next step of the iteration this modified electric field distribution is applied. After a few consecutive iterations a self-consistent electric field distribution is obtained. (In one step of the iteration typically $N=10\,000-50\,000$ electrons are released from the cathode.)

IV. RESULTS AND DISCUSSION

Figure 3 shows the measured voltage-pressure characteristics of the discharge at $i=1$, 2, and 3 mA discharge current. The sharp rise of the discharge voltage (characterizing the obstructed regime) around $p=6$ mbar pressure can be clearly observed.

Most of the discharge simulations have been carried out for the $i=1$ mA graph presented in Fig. 3. An anode-cathode distance $L=0.46$ cm, as in the experimental discharge tube, was used throughout the simulations. The effectiveness of our iteration process is demonstrated in Fig. 4. Figure 4 shows the self-consistent electric field distribution where the iteration was started from two different initial field distributions. It can be seen that the convergence of the iteration is rather fast, the second iterations for both of the initial distributions already agree within the thickness of the line.

The electric field distributions calculated this way are plotted in Fig. 5 for different helium pressures in the range of $p=5.9-7$ mbar. Measured voltage-pressure data points for pressures higher than 7 mbar resulted in a vanishing electric field at the anode, and these data points were excluded from further investigations. Our results suggest a possible definition of the obstructed discharge, i.e., where *the electric field does not vanish at the anode.* The distribution of the electric field changes remarkably with changing the pressure. At lower pressures (i.e., in the highly obstructed range), the electric field distribution

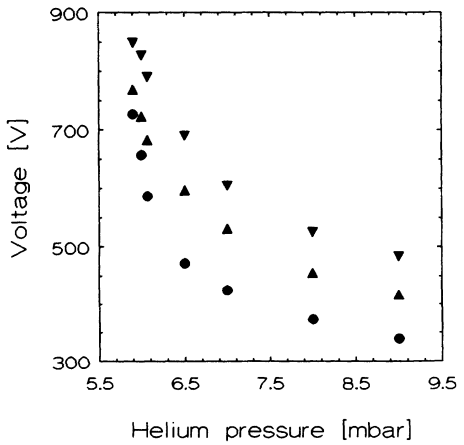

FIG. 3. Voltage-pressure characteristics of the discharge at a current of (●) $i=1$ mA, (▲) $i=2$ mA, and (▼) $i=3$ mA.

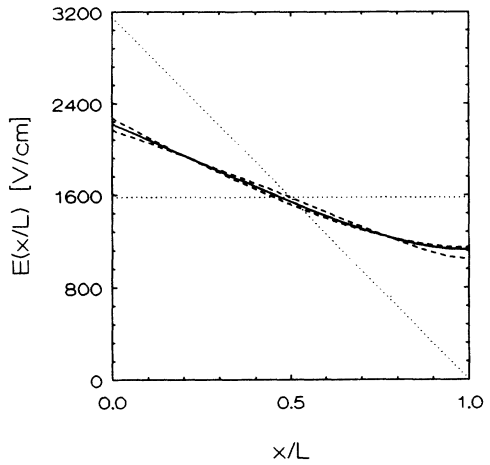

FIG. 4. The iterated electric field distribution starting from two different initial field distributions. Discharge parameters: $V=727$ V, $j=0.32$ mA/cm^2, $p=5.9$ mbar, and $L=0.46$ cm. (. . . . initial distribution, — — — first iterate, —— second iterate of the electric field distribution.)

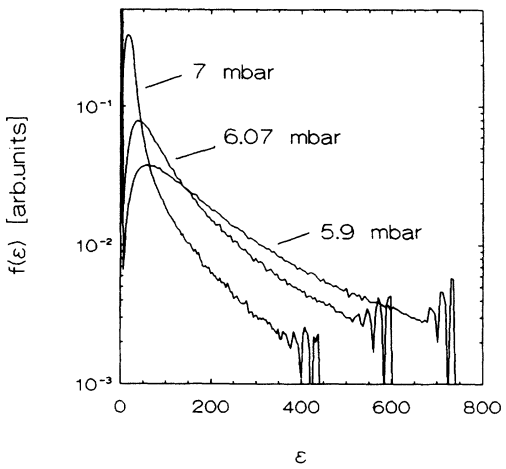

FIG. 6. The energy distribution of electrons absorbed by the anode at different helium pressures. (Current density: $j=0.32$ mA/cm^2, the discharge voltage was 425 V at 7 mbar, 585 V at 6.07 mbar, and 727 V at 5.9 mbar.)

changes less. While at 7 mbar pressure, there is only a low electric field of approximately 100 V/cm at the anode; at 5.9 mbar, this value rises up to about 1200 V/cm field strength.

The energy spectra of electrons absorbed by the anode are plotted in Fig. 6 for selected values of helium pressure. The increasing discharge voltage, together with a decreasing pressure in the obstructed regime, may result in the "runaway effect" of electrons. Many high-energy electrons are absorbed by the anode, which in a wider discharge gap would have otherwise produced more ions.

Figure 7 shows the spatially averaged energy distribution of ionizing electrons. The data were obtained in the following way: whenever an ionization process occurred in the simulation, the energy of the incoming (ionizing) electron was memorized regardless of the position. Finally, the energy distribution was calculated. It can be seen from Fig. 7 that a considerable amount of the ionization is caused by the high-energy electrons. The electron impact ionization cross section of helium peaks around 120 eV energy. The number of ionizations by electrons having a higher energy than 120 eV can be compared to the total number of ionizations. The results of the calculations are also presented in Table I. The share of the high-energy electrons in ion production (H) increases with decreasing pressure, i.e., with increasing discharge voltage.

Table I also shows the electron multiplication data for the given discharge conditions. It was expected that the multiplication should be approximately the same in all cases since, in the range of discharge parameters (voltage, pressure) investigated, the γ_i secondary electron emission coefficient is constant. (In the obstructed regime, the electron emission from the cathode due to positive ion bombardment is believed to give the dominant contribution to the maintenance of the discharge.) The systematic increase in the multiplication may be explained as follows. At higher electric fields the motion of electrons

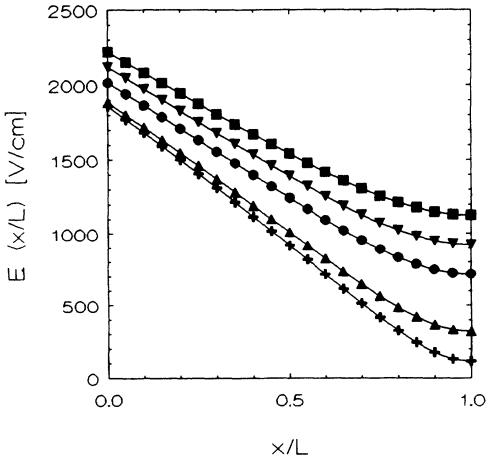

FIG. 5. The self-consistent electric field distribution calculated from the model for different helium pressures at $j=0.32$ mA/cm^2 current density (+, 7 mbar; ▲, 6.5 mbar; ●, 6.07 mbar; ▼, 6 mbar; and ■, 5.9 mbar).

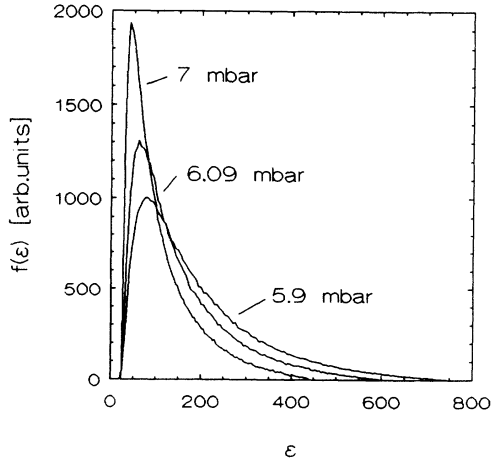

FIG. 7. The spatially averaged energy distribution of ionizing electrons at $p=7$, 6.09, and 5.9 mbar helium pressure at $j=0.32$ mA/cm^2 current density.

TABLE I. Discharge parameters: p, pressure; V, voltage; H, the percentage of ionizing collisions, where the ionizing electron had a kinetic energy higher than 120 eV; and M, electron multiplication. (Current density: $j=0.32$ mA/cm^2.)

p (mbar)	V (V)	H (%)	M
5.9	727	62	9.3
6.0	657	56	9.8
6.07	587	50	10.4
6.5	472	38	12.0
7	425	32	13.4

and ions is directed more along the field lines. At the lowest possible pressure of $p=5.9$ mbar, the multiplication was found to be $M=9.3$ (meaning in an average sense $M-1=8.3$ ions created per one emitted electron), which is still enough to satisfy the self-maintenance criteria of the discharge. The additional ions created at higher pressures are supposedly lost by recombination at the wall of the discharge tube.

Studies of the cathode region of (abnormal) glow discharges indicate that the electron impact ionization rate peaks near the cathode dark-space–negative-glow boundary (see, e.g., [18]). In our "slightly" obstructed discharge at $p=7$ mbar, this peak of (dn^+/dt) can be still observed at about $x/L=0.85$. At lower pressures the position of the peak shifts towards the anode. At sufficiently low pressures, the peak disappears and the maximum of (dn^+/dt) occurs at the anode $(x/L=1)$. This happens at $p=6.09$ and 5.9 mbar as indicated in Fig. 8.

A. Electric field measurements

The light emitted from the discharge in the obstructed regime is at a quite low level. Therefore, a somewhat higher current density discharge was established to obtain a usable light intensity for the electric field measurements. The results of the measurements are shown in Figs. 9 and 10. Figure 9 illustrates the curve-fitting procedure and shows the measured line shape of the H_δ ($\lambda=401.2$ nm) spectral line recorded at the position $x/L=0.7$ (at $V=1020$ V discharge voltage, $j=0.8$ mA/cm^2 current density, and $p=5.7$ mbar helium pressure), and the result of the curve-fitting procedure. Figure 10 shows the data obtained from the electric field measurements together with the self-consistent electric field distribution calculated from the model using the same conditions as in the experiment. The measured Stark split line shapes of the H_δ spectral line at different positions are also indicated. There is a fairly good agree-

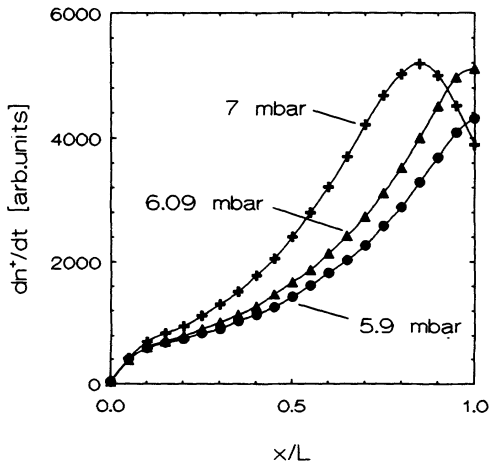

FIG. 8. The spatial distribution of the He^+ ion production at $p=7$, 6.09, and 5.9 mbar helium pressure at $j=0.32$ mA/cm^2 current density.

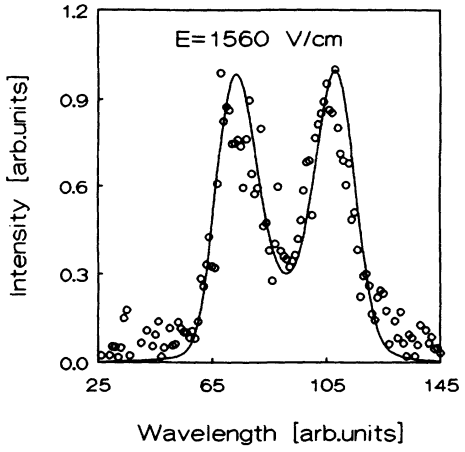

FIG. 9. The measured line shape of the H_δ ($\lambda=401.2$ nm) spectral line (○) at the position $x/L=0.7$ and the result of the curve fitting (——). (Discharge voltage, $V=1020$ V; current density, $j=0.8$ mA/cm^2; and helium pressure, $p=5.7$ mbar.) The wavelength is measured in arbitrary units with respect to the start of the recording.

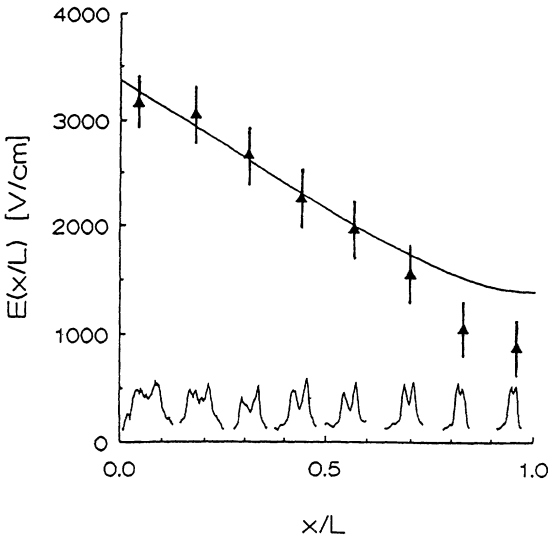

FIG. 10. Calculated self-consistent electric field distribution (——) and data determined from Stark measurements (▲). The measured Stark split line shapes of the H_δ spectral line at different positions are also indicated. (Experimental and simulated discharge conditions: discharge voltage, $V=1020$ V; current density, $j=0.8$ mA/cm^2; and helium pressure, $p=5.7$ mbar.)

TABLE II. Discharge parameters calculated at different values of the electrode reflection R. H, the percentage of ionizing collisions, where the ionizing electron had a kinetic energy higher than 120 eV; and M, electron multiplication. ($V=727$ V, $j=0.32$ mA/cm^2, $p=5.9$ mbar.)

R	H (%)	M
0.0	62	9.3
0.1	58	11.4
0.2	54	14.4

ment between the measured and the calculated field distribution.

B. Effect of electrode reflection

Experimental measurements on backscattering of low-energy electrons from carbon show that the backscattering coefficient ranges between 0.05 and 0.44 [22]. We have carried out a simple study where the discharge characteristics were calculated at a given set of conditions (voltage, current density, and pressure) at three different values of the reflection coefficient (at both anode and cathode), which (as a simplification) was assumed to be energy independent. It was found that some discharge parameters, such as the multiplication, are sensitive to the value of the reflection coefficient. Table II includes the data obtained for $V=727$ V, $j=0.32$ mA/cm^2, $p=5.9$ mbar, at reflection coefficients of $R=0$, 0.1, and 0.2.

It can be seen from Table II that the share of high-energy electrons in ion production (H) is decreasing slightly at higher values of R. The spatial distribution of ionizations is also significantly changed by introducing the reflective electrodes. Especially at the vicinity of the anode, the ion production is largely enhanced as can be seen in Fig. 11. The increased ion production also results in an increased ion density and, consequently, the electric field changes more rapidly (see Fig. 12).

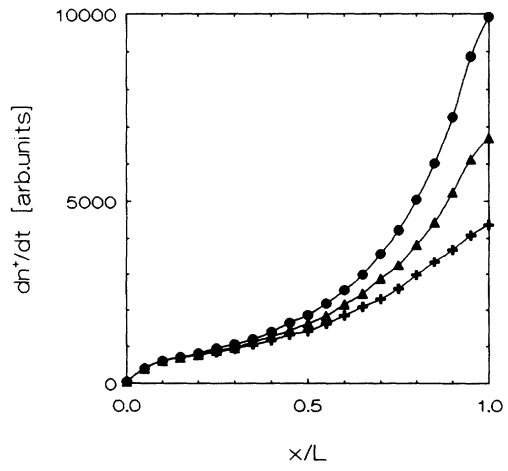

FIG. 11. The spatial distribution of the He^+ ion production at different values of the electrode reflection R. (+, $R=0$; ▲, $R=0.1$; and ●, $R=0.2$.) (Discharge conditions: $V=727$ V, $j=0.32$ mA/cm^2, and $p=5.9$ mbar.)

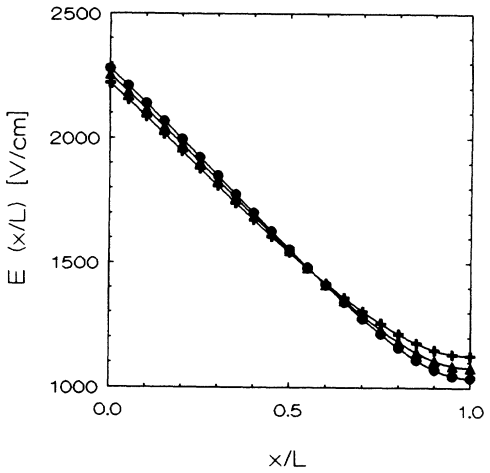

FIG. 12. The calculated self-consistent electric field distribution at different values of the electrode reflection R. (+, $R=0$; ▲, $R=0.1$; and ●, $R=0.2$). (Discharge conditions: $V=727$ V, $j=0.32$ mA/cm^2, and $p=5.9$ mbar.)

V. CONCLUSIONS

An obstructed glow discharge in helium was investigated. The voltage-current characteristics of the discharge have been measured and the spatial distribution of the electric field was also determined by spectroscopic measurements. A model of the discharge was developed and several discharge characteristics (electron multiplication, energy distribution of electrons absorbed by the anode, energy distribution of ionizing electrons, share of high-energy electrons in ion production, and spatial distribution of ion production) were calculated for different pressures. The corresponding voltage and current density values were taken from experimental data.

The self-consistent electric field distribution in the discharge gap was also calculated from the model and the results obtained in this way showed a good agreement with the experimentally determined electric field distribution.

We have calculated the electric field distribution at different gas pressures. The results indicated that towards the lower pressures, where the discharge is "more obstructed," the electric field distribution tends to be more homogeneous (at constant current density). The study of the energy spectra of electrons absorbed by the anode showed that with decreasing pressure more high-energy electrons reach the anode. The contribution of the high-energy electrons to the He^+ production increased with decreasing pressure and increasing voltage. Electrons with an energy higher than 120 eV make a major contribution to the ion production, especially in the strongly obstructed regime. The spatial distribution of the ion production showed that most of the ions are created near the anode. This indicates that, if the elec-

trode separation (or the gas pressure) is increased, there is a great difference in the overall ion production. This observation can explain why the obstructed discharge is very sensitive to minor changes in gas pressure.

The effect of electron reflection from the electrodes was also studied. The reflecting electrodes significantly enhanced the ion production rate (especially near the anode). The electric field distribution was found to be slightly different due to the increased ion density resulting from the greater ion production rate.

ACKNOWLEDGMENTS

The authors thank Professor A. V. Phelps, Professor A. Gallagher, Doctor B. Jelenković (JILA, University of Colorado), Doctor M. Jánossy, and Doctor P. Apai (Research Institute for Solid State Physics) for helpful discussions, and T. J. Forgács, J. Tóth, E. Sárközi, and Gy. Császár for the construction of the discharge tube. This work was supported by OTKAF-4475 and T-2935 Grants and by the Australian Research Council (RCT).

[1] A. Güntherschulze, Z. Phys. **61**, 581 (1930).
[2] F. M. Penning, Phys. Z. **33**, 816 (1932).
[3] G. Francis, *Encyclopedia of Physics* (Springer, New York, 1956), Vol. XXII, p. 53.
[4] A. von Engel, *Ionized Gases* (Clarendon, Oxford, 1965).
[5] D. K. Doughty and J. E. Lawler, Appl. Phys. Lett. **42**, 234 (1983).
[6] B. N. Ganguly and A. Garscadden, J. Appl. Phys. **70**, 621 (1991).
[7] J. Stark, *Handbuch der Experimentalphysik* (Akademische Verlag, Leipzig, 1927).
[8] C. Barbeau and J. Jolly, in *International Meeting on Optogalvanic Spectroscopy, Glasgow,* edited by R. S. Stewart and J. E. Lawler, IOP Conf. Proc. No. 113 (Institute of Physics, London, 1990), p. 65.
[9] C. Barbeau and J. Jolly, Appl. Phys. Lett. **58**, 237 (1991).
[10] E. Schrödinger, Ann. Phys. **80**, 437 (1926).
[11] J. P. Boeuf and E. Marode, J. Phys. D **15**, 2169 (1982).
[12] D. B. Graves and M. Surendra, in *Nonequilibrium Effects in Ion and Electron Transport,* edited by J. W. Gallagher (Plenum, New York, 1990), p. 157.
[13] J. P. Boeuf and E. Marode, in *Proceedings of the XVI ICPIG (International Conference on Phenomena in Ionizad Gases), Düsseldorf, Invited Papers,* edited by W. Bötticher, H. Wenk, and E. Schulz-Gulde (University of Düsseldorf, Düsseldorf, 1983), p. 206.
[14] H. D. Hagstrum, Phys. Rev. **104**, 317 (1956).
[15] L. N. Labahn and J. Callaway, Phys. Rev. A **2**, 366 (1970).
[16] F. J. de Heer and R. H. J. Jansen, J. Phys. B **10**, 3741 (1977).
[17] F. J. de Heer, R. H. J. Jansen, and W. van der Kaay, J. Phys. B **12**, 979 (1979).
[18] E. A. Den Hartog, D. A. Doughty, and J. E. Lawler, Phys. Rev. A **38**, 2471 (1988).
[19] O. B. Firsov, Zh. Eksp. Teor. Fiz. **21**, 1001 (1951).
[20] D. Rapp and W. E. Francis, J. Chem. Phys. **37**, 2631 (1962).
[21] S. Sinha and J. N. Bardsley, Phys. Rev. A **14**, 104 (1976).
[22] R. L. Verma, J. Phys. D **10**, 1167 (1977).